ACS APPLIED MATERIALS & INTERFACES

Research Article

www.acsami.org

Direct Determination of Field Emission across the Heterojunctions in a ZnO/Graphene Thin-Film Barristor

Edmund M. Mills,[†,⊥] Bok Ki Min,[‡,∥,⊥] Seong K. Kim,[†] Seong Jun Kim,[‡] Min-A Kang,[‡] Wooseok Song,[‡] Sung Myung,[‡] Jongsun Lim,[‡] Ki-Seok An,*[,‡] Jongwan Jung,[†,§] and Sangtae Kim*[,†]

[†]Department of Chemical Engineering and Materials Science, University of California, Davis, California 95616-5294, United States

[‡]Thin Film Materials Research Group, Korea Research Institute of Chemical Technology (KRICT), Yuseong P.O. Box 107, Daejeon 305-600, Republic of Korea

[§]Graphene Research Institute, Department of Nanoscience and Technology, Sejong University, 98 Gunja-dong, Gwangjin-gu, Seoul 143-747, Republic of Korea

[∥]Department of Physics, Sungkyunkwan University, 2066 Seoburo, Jangan-gu, Suwon, Gyeonggi-do 440-746, Republic of Korea

Supporting Information

ABSTRACT: Graphene barristors are a novel type of electronic switching device with excellent performance, which surpass the low on−off ratios that limit the operation of conventional graphene transistors. In barristors, a gate bias is used to vary graphene's Fermi level, which in turn controls the height and resistance of a Schottky barrier at a graphene/semiconductor heterojunction. Here we demonstrate that the switching characteristic of a thin-film ZnO/graphene device with simple geometry results from tunneling current across the Schottky barriers formed at the ZnO/graphene heterojunctions. Direct characterization of the current−voltage−temperature relationship of the heterojunctions by ac-impedance spectroscopy reveals that this relationship is controlled predominantly by field emission, unlike most graphene barristors in which thermionic emission is observed. This governing mechanism makes the device unique among graphene barristors, while also having the advantages of simple fabrication and outstanding performance.

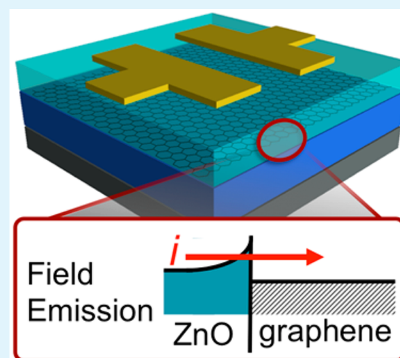

KEYWORDS: *graphene, barristors, schottky barriers, field emission, ac impedance spectroscopy*

1. INTRODUCTION

Graphene is an excellent conductor with high electron and hole mobility. It is transparent and flexible, and has exceptional mechanical strength.[1] Over the past decade, graphene's unique electrical properties have prompted extensive research into its use in a wide variety of electronic devices, including barristors,[2] solar cells,[3] photodiodes,[4] and gas sensors.[5] Many of these devices make use of a Schottky barrier (SB) formed at a heterojunction between a semiconductor and the metallic graphene. Therefore, understanding the electrical characteristics of such SBs is an essential step in the design and optimization of these advanced graphene devices.

We recently reported the fabrication of a simple ZnO/graphene two-dimensional thin-film device exhibiting switching behavior with both a high on−off ratio (10^5) and excellent carrier mobility (329.7 ± 16.9 $cm^2\ V^{-1}\ s$).[6] Conventional ZnO thin-film transistors (TFTs) often suffer from relatively low carrier mobility, while the performance of typical graphene TFTs is largely limited by the metallic nature of graphene. These TFTs operate through the formation of a channel with a high density of charge carriers induced by a gate bias. However, we believe that the unique switching characteristic of our device originates from current passing across a series of ZnO/graphene heterojunctions, as in graphene barristors.[2,7] In graphene barristors, a gate bias is used to modulate graphene's work function, which is directly linked to the height of the SB.[8,9] The barrier height and the current across it follow a reverse exponential relationship under thermionic emission (TE) where thermal energy excites charge carriers over the SB (Table 1).[2,7] This allows for the high on−off ratios achieved in graphene barristors (e.g., 10^5),[2] overcoming the primary limitation of conventional graphene transistors.[10]

In the present study, we investigate the origin of the transistive behavior of such ZnO/graphene devices with in-depth characterization using ac-impedance spectroscopy (IS) and provide detailed mechanistic information about the current across the ZnO/graphene heterojunctions within the device.[11] As will be demonstrated below, the SBs formed at the junction indeed control the device's overall electrical response. Interestingly enough, the current across the SBs predominantly follows field emission (FE), in which the charge carriers transverse the SB by tunneling. This is in contrast to previously studied graphene barristors and other devices, where the current almost exclusively follows TE.[2,5,7,9,12−14]

Received: April 18, 2015
Accepted: July 20, 2015
Published: July 20, 2015

ACS Publications © 2015 American Chemical Society

DOI: 10.1021/acsami.5b03380
ACS Appl. Mater. Interfaces 2015, 7, 18300−18305

Table 1. Temperature Dependence of V_o in the $I-V$ Relationship $I = I_o \exp(V/V_o)$ for TE, TFE, and FE, As Determined by Padovani and Stratton[17,a]

	Forward Bias	Reverse Bias
Thermionic Emission	$V_o = V_{th} = \frac{k_B T}{q}$	$I = I_o = AA^*T^2 \exp\left(\frac{\phi_B}{V_{th}}\right)$[b]
	$I_o = AA^*T^2 \exp\left(\frac{\phi_B}{V_{th}}\right)$	
Thermionic Field Emission	$V_o = \frac{E_0}{q} = \frac{E_{00}}{q} \coth\left(\frac{E_{00}}{qV_{th}}\right)$	$V_o = \varepsilon' = \frac{E_{00}}{q}\left[\frac{E_{00}}{qV_{th}} - \tanh\left(\frac{E_{00}}{qV_{th}}\right)\right]$
Field Emission	$V_o = \frac{E_{00}}{q} = \frac{\hbar}{2}\sqrt{\frac{N}{\varepsilon_0 \varepsilon_r m^*}}$	$I = I_o \frac{\exp(-2\phi_B c_1/3)}{c_1(V)\sin(\pi k T c_1)}$[c]
		$c_1 = \frac{1}{E_{00}}\sqrt{\frac{\phi_B}{(\phi_B + \lvert V \rvert)}}$

[a] A, A^*, V_{th}, ϕ_B, E_{00}, E_0, N, ε_r, and m^* are the interface area, Richardson constant, thermal voltage, SB height, two tunneling parameters, impurity concentration, relative dielectric constant of ZnO, and effective electron mass in the ZnO, and k_B, T, q, $\hbar$, and ε_0 have their usual meanings. [b,c] Under reverse bias, TE and FE do not follow an exponential relationship, so the full expression for the $I-V$ relationship is given.

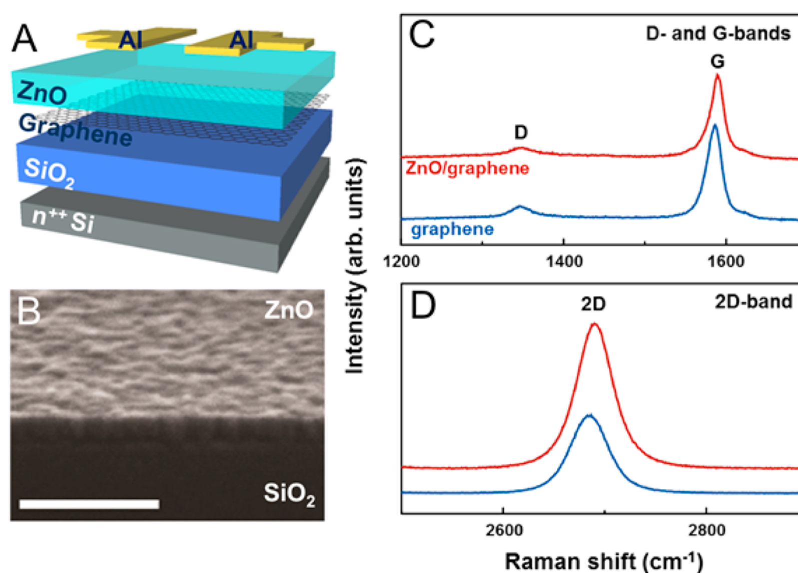

Figure 1. (A) Schematic of the ZnO/graphene device. (B) SEM cross-sectional image of the ZnO/graphene device, showing a 60 nm thick polycrystalline ZnO film. (Scale bar is 500 nm). (C, D) Raman spectra recorded with an excitation wavelength of 514 nm of (C) the D- and G-bands and of (D) the 2D-bands for pristine graphene and ZnO/graphene hybrid films. This shows the successful synthesis of single layer graphene, and its incorporation into the device.

2. RESULTS

2.1. ZnO/graphene barristor. A schematic of the ZnO/graphene barristor studied in this work is shown in Figure 1(A). The device is very simple; it is composed of a layer of graphene sandwiched between a ZnO thin film and SiO_2/Si substrate, with aluminum electrodes on the surface for electrical contact. A representative cross-sectional view image of ZnO/graphene taken using a scanning electron microscopy (SEM) technique is shown in Figure 1(B). From the image, the film thickness was estimated to be ~60 nm. X-ray powder diffraction (XRD) patterns of the ZnO/graphene device and the reference ZnO thin films exhibit the hexagonal wurtzite phase (Figure S1). The (100), (002), and (101) peaks clearly appear in the pattern, indicating that the ZnO films are in a polycrystalline form. Raman spectra for both pristine graphene samples and the ZnO/graphene device are shown in Figure 1(C, D). The characteristic graphene fingerprints, including the D-, G-, and 2D-bands, were observed for all samples. The intensity ratio of the 2D- and G-bands can be used to determine the number of layers of graphene present, in this case indicating the presence of predominantly single layer graphene. The similarity between the Raman spectra of the pristine graphene and the ZnO/graphene device indicates that the graphene is not damaged and does not undergo chemical reaction during the deposition of the ZnO layer.

The results of the X-ray photoelectron spectroscopy (XPS) depth profile measurements are shown in Figure S2. Like Raman spectroscopy, XPS shows that the graphene is preserved with ZnO deposition, as the spectrum obtained from ZnO/graphene is similar to that of the graphene reference sample, and is consistent with those of graphene previously reported.[15] Peaks corresponding to the graphene-related sp^2 C−C bond and small peaks corresponding to C−O and C=O bonds were observed at the ZnO/graphene interface, showing the

DOI: 10.1021/acsami.5b03380
ACS Appl. Mater. Interfaces 2015, 7, 18300−18305

formation of an abrupt interface between the graphene and ZnO thin film. No evidence of PMMA residue from the transfer process was observed. Carbon contamination was observed only at the outermost surface. The SEM, XRD, Raman spectroscopy, and XPS characterization unambiguously demonstrate that the ZnO/graphene device is composed of a 60 nm thick polycrystalline ZnO thin film on a highly crystalline single layer of graphene, with a sharp interface between the two.

In this device, we expect that, due to the high conductance of the graphene layer compared to the ZnO film, current will pass through the ZnO film, across the ZnO/graphene heterojunction, and through the graphene before crossing the interface and ZnO film again. It should also be noted that, as indicated in Figure 2, the current crosses two heterojunctions in series. This has implications for the analysis of the heterojunction,[16] which will be discussed further on.

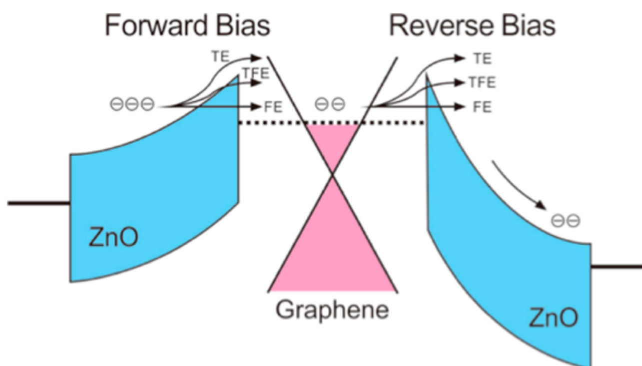

Figure 2. Barristor includes two serial SBs, with opposite orientation to the direction of current. Regardless of the direction of applied bias, one of the SBs will be under forward bias and the other will be under reverse bias. TE, TFE, FE mechanisms are shown with arrows.

2.2. Characterization Using AC-Impedance Spectroscopy.

IS was then used to characterize this device, including the ZnO/graphene SB.[11] The primary advantage of IS for this purpose over dc current−voltage ($I-V$) measurements is the possibility of separating the local impedances of different sample elements, whereas dc measurements give the total resistance of the sample. This is made possible by the use of the frequency domain: the frequency-dependence of the charge carrier relaxation varies with local charge transfer characteristics. This unique capability of IS allows more detailed characterization of the behavior of particular device elements than is possible with dc techniques. Until recently,[11] the use of IS for the characterization of graphene-based electrical devices was rare, though it has been widely used for the characterization of electrochemical devices such as graphene supercapacitors.

The impedance of the ZnO/graphene barristor was measured with a simultaneously applied DC bias from 0 to 3 V at room temperature, plotted in Figure 3 as Cole−Cole plots. These appear as single semicircles, the x-intercept of which reduces with bias. By comparing the Cole−Cole plots to those simulated by an appropriate equivalent circuit, the local resistances and capacitances in the device can be determined. The equivalent circuit which we believe the most appropriate for the device is shown in the inset in Figure 3. It takes the ZnO/graphene junctions as a resistor and capacitor in parallel (R_{SB} and C_{SB}), the graphene as a resistor (R_g), and the SiO_2 layer of the substrate as a capacitor (C_{sub}), consistent with the device's expected current path described earlier. With the proposed equivalent circuit, the impedance of the device is given by eq 1

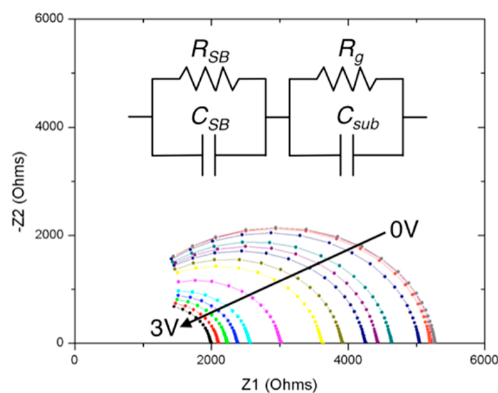

Figure 3. IS was used to characterize the ZnO/graphene device with simultaneously applied dc bias from 0 to 3 V. The spectra collected at room temperature are plotted as a Cole−Cole plot. With increasing bias, the x-intercept, indicating the total resistance of the device, decreases. The spectra were fit to the equivalent circuit shown above, to extract the resistance and capacitance of the ZnO/graphene heterointerface (R_{SB} and C_{SB}), the resistance of the graphene (R_g), and the capacitance of the substrate (C_{sub}).

$$Z_t(\omega) = \left(\frac{1}{R_{SB}} + j\omega C_{SB}\right)^{-1} + \left(\frac{1}{R_g} + j\omega C_{sub}\right)^{-1} \quad (1)$$

where $Z_t(\omega)$ is the complex impedance of the device and ω is the frequency of the ac current. In a Cole−Cole plot, a resistor (R) and capacitor (C) in parallel appears as a semicircular arc with peak frequency ω' and characteristic relaxation time τ given by $\omega' = \tau^{-1} = 1/RC$. The Cole−Cole plot of Z_t is expected to consist of two such semicircular arcs with different peak frequencies. However, because of the limiting frequency range of the analyzer used for the measurements, only a single arc is observed. The best fit of the plot at zero bias with the impedance of the equivalent circuit gave R_g, C_{sub}, R_{SB}, and C_{SB} as $1260 \pm 80\ \Omega$, $7.4 \pm 0.3 \times 10^{-10}$ F, $4000 \pm 80\ \Omega$, and $3.1 \pm 0.3 \times 10^{-10}$ F, respectively.

To confirm the proposed current path and equivalent circuit model, we compare the local resistance of the ZnO/graphene device to those of independently measured graphene and ZnO thin films. To this end, the impedance of graphene/SiO_2/Si and ZnO/SiO_2/Si samples were prepared and characterized with IS. The geometries of these samples were identical to that of the barristor. In the graphene sample, the graphene resistance is measured to be ~1 kΩ, consistent with R_g of the ZnO/graphene device. The lateral resistance of the ZnO thin film was found to be much higher (55 kΩ), supporting the earlier proposition that current will flow through the graphene rather than the ZnO in the device. The resistance across the ZnO layer is calculated to be less than 1 Ω, consistent with our equivalent circuit model from which this resistance is omitted.

2.3. Current−voltage relationship of the heterojunction.

Now we provide in-depth discussion on the electrical characteristics of the ZnO/graphene heterojunction. We will show that a SB is formed at the heterojunction and that current across it follows FE, by examining the bias and temperature dependence of R_{SB}.

The $I-V$ relationship of the ZnO/graphene heterojuction can be calculated from the R_{SB} determined as a function of

DOI: 10.1021/acsami.5b03380
ACS Appl. Mater. Interfaces 2015, 7, 18300−18305

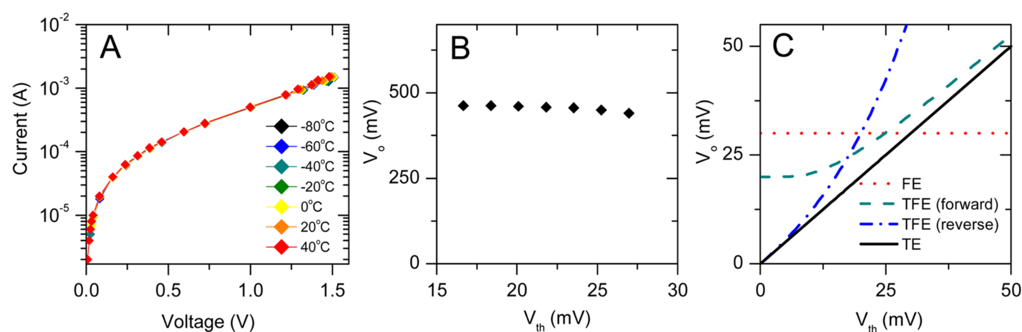

Figure 4. (A) The semilogarithmic plot of the current−voltage relationship is linear above ~0.4 V, indicating exponential behavior. The current−voltage behavior is temperature independent. (B) V_o, from the slope of the linear region in the semilogarithmic plot, is plotted against V_{th}. (C) V_o varies differently with temperature for TE, TFE, and FE. Examining the temperature dependence of V_o allows the identification of the current mechanism across a SB.

applied bias. The voltage drop across the heterojuction is given by eq 2,

$$V_i = V\left(\frac{R_{SB}}{R_{SB} + R_g}\right) \tag{2}$$

and the current reads

$$I = \frac{V_{SB}}{R_{SB}} = \frac{V}{(R_{SB} + R_g)} \tag{3}$$

This is plotted in the semilogarithmic plot shown in Figure 4(A), in the temperature range of −80 to +40 °C.

3. DISCUSSION

In general, there are three primary types of electron transport across SBs (i.e., thermionic emission (TE), thermionic field emission (TFE), and field emission (FE)), each of which has different $I-V$ characteristics. Briefly, in TE the charge carrier hops over the barrier, excited by thermal energy, as previously mentioned. In FE, on the other hand, the charge carrier tunnels directly through the barrier. TFE is a combination, where the charge carrier is excited by thermal energy to a potential where the barrier is thin enough for tunneling to take place. These different mechanisms are represented in Figure 2. For each, the current across the SB is roughly exponential and is given by eq 4,

$$I = I_o \exp\left(\frac{V}{V_o}\right) \tag{4}$$

where I_o is a saturation current that shows only minor variation with applied bias. I_o and V_o are different for each model and vary differently with temperature, so which mechanism of current transport is at play can be determined by the temperature dependence of V_o. The expressions for V_o for each model are summarized in Table 1, from the analysis by Padovani and Stratton.[17] The $I-V$ relationships of both TE and FE do not follow the exponential relationship of eq 4 under reverse bias, and thus, the $I-V$ relationship is given rather than V_o. The simulated temperature dependence of V_o for each model is plotted in Figure 4(C), using selected values for the different parameters.[18] In this method of identifying the current mechanism, image-force barrier lowering and the change in SB height of graphene SBs under reverse bias[5,19] have been ignored, as these will only slightly modify the overall $I-V$ characteristics.

The $I-V$ curve measured exhibits an exponential relationship above ~0.4 V (Figure 4(A)). The slope of the semilogarithmic plot in this region is V_o, which has been plotted vs temperature in Figure 4(B). Similar to the relationship shown for FE over a forward-biased SB in Figure 4(C), V_o is temperature independent, which indicates that the current follows FE and that R_{SB} is predominantly controlled by the forward-biased SB.

The dominance of the resistance of one barrier over the other is not surprising: as the $I-V$ relationships under forward and reverse bias are different, the potential drop will split unevenly between the two junctions, keeping the current across each identical. Typically, SBs formed at such heterojunctions are rectifying, so that the current differs by orders of magnitude under forward and reverse bias of equivalent magnitude. For serial SBs oppositely oriented, the potential drop is often concentrated across one of the SBs, and thus, the $I-V$ behavior is determined by the limiting, higher resistance SB. As previously mentioned, in the present case the forward-biased SB controls R_{SB}, which allows this simple device to serve as an excellent barristor.

The use of this device as a barristor requires a strong dependence of the current on the SB height, so that a large on−off ratio is achieved by varying the SB height with a gate bias. The saturation current (I_o) for tunneling through a SB under FE and forward bias is given by eq 5,[17]

$$I_o = \frac{2\pi AA^* \exp\left(-\frac{\phi_B}{E_{00}}\right)}{k_B T \log\left[\frac{2(\phi_B - V)}{\xi_2}\right] \sin\left\{\frac{\pi k_B T}{2E_{00}} \log\left[\frac{2(\phi_B - V)}{\xi_2}\right]\right\}} \tag{5}$$

where ξ_2 is the difference between the Fermi level of the semiconductor and the bottom of the conduction band. As in TE, in FE the current and SB height are related exponentially, leading to the device's high on−off ratio.

The observation of a FE mechanism is unusual among previous studies of ZnO/graphene heterojunctions, which primarily report a TE mechanism.[8,20−22] There is one case where TFE is observed at the contact of graphene and a ZnO nanorod, where tunneling is favored because of the large current density.[23] To understand the dominance of tunneling current across the heterojunction in our device, we consider the effect of the impurity concentration N in the ZnO thin film. The expression relating N and V_o for FE is shown in Table 1. It was calculated that E_{00} = 0.45 eV and, using the theoretical m^* of 0.28 × m_e for ZnO, N = 1.39 × 10^{21} cm^{-3}. With such a high N, the SB becomes very thin, encouraging tunneling as the

DOI: 10.1021/acsami.5b03380
ACS Appl. Mater. Interfaces 2015, 7, 18300−18305

predominant transport mechanism. To verify the high N, Hall effect measurements were carried out on the ZnO thin film sample and the charge carrier concentration is determined to be 1.35×10^{21} cm^{-3}, in excellent agreement with the value of N we found previously using the FE model. We note that the unusually large lateral resistance of the ZnO thin film (55 kΩ) with such a high N is attributed to resistive grain boundaries in the polycrystalline film. These results confirm that FE is the governing mechanism of the ZnO/graphene heterojunction.

4. CONCLUSION

In summary, a simple ZnO/graphene barristor was directly characterized by IS. We have demonstrated that the switching characteristic of the device is uniquely governed by field emission such that tunneling is predominantly responsible for the current across the heterojunction of ZnO/graphene. From the $I-V$ relation, a large impurity concentration in the ZnO was calculated using the FE model, which was consistent with that independently determined by Hall measurements. Our results have clearly demonstrated that FE is an equally viable mechanism for graphene barristors to the usual TE mechanism.

5. METHODS

5.1. ZnO/graphene thin-film device fabrication. Graphene was synthesized on 25 μm-thick Cu foils (Sigma-Aldrich) by thermal chemical vapor deposition (TCVD). The Cu foil was put into a quartz tube and preannealed under 2 Torr H_2 (100 sccm) at 1050 °C for 30 min, after which a mixture of CH_4 (2 sccm) and H_2 (100 sccm) was introduced for 20 min to synthesize graphene films. The samples were cooled down to room temperature. The synthesized graphene films were then transferred onto heavily p-doped silicon (100) substrates with a 300 nm SiO_2 surface layer by a poly(methyl methacrylate) (PMMA) assisted wet transfer method. The substrates were cleaned beforehand in deionized water containing detergent, acetone, and isopropanol by ultrasonication.

Atomic layer deposition (ALD) was used to deposit ZnO films. Diethylzinc (DEZ) was employed as a precursor for ZnO in combination with H_2O as an oxidant. Before DEZ exposure, the working pressure in a reaction chamber was kept at 3 Torr with Ar gas (purity 99.999%). The DEZ vapor contained in a stainless-steel bubbler was delivered to the chamber at room temperature by Ar carrier gas. The flow rate of the carrier gas was controlled using a mass flow controller. Water vapor was introduced to the chamber without using a carrier gas. A single cycle of the process consisted of DEZ exposure for 0.3 s, Ar purging for 10 s, water vapor exposure for 1 s, and another Ar purging for 10 s, sequentially. The cycle was repeated 300 times (300 cycles) to deposit a ZnO film on the graphene sheet.

The source/drain electrodes were fabricated by thermally deposing aluminum (100 nm) on the ZnO film surface using a shadow mask to fabricate the ZnO/graphene thin film device.

5.2. Device characterization. Raman spectra of pristine graphene and the ZnO/graphene device were obtained using a Raman spectrometer (Renishaw) with excitation wavelength of 514 nm to verify the successful synthesis of graphene and its incorporation into the device, and also to determine the number of layers of graphene.

SEM images of the ZnO film over graphene were taken using a Cryo-FE-SEM (TESCAN Mira 3 LMU FEG) with accelerating voltage of 20 kV, from which the ZnO film thickness was determined.

The crystallinity of the ZnO thin films was studied by XRD performed on a Rigaku D/Max-2200 diffractometer with Cu Kα radiation.

The chemistry of the ZnO/graphene interface was investigated using XPS spectra, acquired with a normal emission geometry using conventional monochromatic Al Kα radiation (h_ = 1486.6 eV) with pass energy of 50 eV. Ar^+ ions etching for depth profiling was used to obtain the XPS depth profile.

5.3. Electrical characterization. All room temperature impedance measurements were performed using an Agilent 4284A impedance analyzer. Measurements were conducted over the frequency range of 10^2 to 10^6 Hz with an AC amplitude of 50 mV, and an applied DC bias in the range of 0−3 V. The variable temperature measurements were performed in vacuum (~10^{-6} Torr) with an MS-tech probe station. Liquid nitrogen and a heating stage were used to control the temperature. The impedance spectra were simultaneously fit using eq 1, employing a custom MATLAB code which used a least-squares method, in order to determine the values of the parameters R_g, C_{sub}, R_{SB}, and C_{SB} as a function of applied bias (V). In the fitting, it was assumed that R_g and C_{sub} did not change with V.

Hall measurements of ZnO films on a SiO_2/Si substrate were carried out at room temperature using a Van der Pauw Ecopia HMS-3000 Hall Measurement System with a standard procedure, to measure the charge carrier concentration of the ZnO thin films.

ASSOCIATED CONTENT

Supporting Information

XRD and XPS depth profile measurements. The Supporting Information is available free of charge on the ACS Publications website at DOI: 10.1021/acsami.5b03380.

AUTHOR INFORMATION

Corresponding Authors

*K.-S.A. e-mail: ksan@krict.re.kr.

*S.K. e-mail: chmkim@ucdavis.edu.

Author Contributions

⊥E.M.M. and B.K.M. contributed equally.

Notes

The authors declare no competing financial interest.

ACKNOWLEDGMENTS

This research was supported by GO! KRICT Project of Korea Research Institute of Chemical Technology, Korea by the R&D Convergence Program of NST (National Research Council of Science & Technology) of Korea, and by a grant (2011-0031636) from the Center for Advanced Soft Electronics under the Global Frontier Research Program of the Ministry of Science, ICT and Future Planning, Korea.

REFERENCES

(1) Geim, A. K. Graphene: Status and Prospects. *Science* **2009**, *324*, 1530−1534.

(2) Yang, H.; Heo, J.; Park, S.; Song, H. J.; Seo, D. H.; Byun, K.-E.; Kim, P.; Yoo, I.; Chung, H.-J.; Kim, K. Graphene Barristor, a Triode Device with a Gate-Controlled Schottky Barrier. *Science* **2012**, *336*, 1140−1143.

(3) Miao, X.; Tongay, S.; Petterson, M. K.; Berke, K.; Rinzler, A. G.; Appleton, B. R.; Hebard, A. F. High Efficiency Graphene Solar Cells by Chemical Doping. *Nano Lett.* **2012**, *12*, 2745−2750.

(4) Fu, X.-W.; Liao, Z.-M.; Zhou, Y.-B.; Wu, H.-C.; Bie, Y.-Q.; Xu, J.; Yu, D.-P. Graphene/ZnO Nanowire/Graphene Vertical Structure Based Fast-Response Ultraviolet Photodetector. *Appl. Phys. Lett.* **2012**, *100*, 223114.

(5) Tongay, S.; Lemaitre, M.; Miao, X.; Gila, B.; Appleton, B. R.; Hebard, A. F. Rectification at Graphene-Semiconductor Interfaces: Zero-Gap Semiconductor-Based Diodes. *Phys. Rev. X* **2012**, *2*, 011002.

(6) Song, W.; Kwon, S. Y.; Jung, M. W.; Kim, S. J.; Min, B. K.; Kang, M.-A.; Kim, S. H.; Lim, J.; An, K.-S. High-mobility Ambipolar ZnO-Graphene Hybrid Thin Film Transistors. *Sci. Rep.* **2014**, *4*, 4064.

(7) Lemaitre, G. M.; Donoghue, E. P.; McCarthy, M. A.; Liu, B.; Tongay, S.; Gila, B.; Kumar, P.; Singh, R. K.; Appleton, B. R.; Rinzler, A. G. Improved Transfer of Graphene for Gated Schottky-Junction, Vertical, Organic, Field-Effect Transistors. *ACS Nano* **2012**, *6*, 9095−9102.

DOI: 10.1021/acsami.5b03380
ACS Appl. Mater. Interfaces 2015, 7, 18300−18305

(8) Lee, S.; Lee, Y.; Kim, D. Y.; Song, E. B.; Kim, S. M. Back-Gate Tuning of Schottky Barrier Height in Graphene/Zinc-Oxide Photodiodes. *Appl. Phys. Lett.* **2013**, *102*, 242114.
(9) Zhong, H.; Xu, K.; Liu, Z.; Xu, G.; Shi, L.; Fan, Y.; Wang, J.; Ren, G.; Yang, H. Charge Transport Mechanisms of Graphene/Semiconductor Schottky Barriers: A Theoretical and Experimental Study. *J. Appl. Phys.* **2014**, *115*, 013701.
(10) Britnell, L.; Gorbachev, R. V.; Belle, B. D.; Schedin, F.; Mishchenko, A.; Georgiou, T.; Katsnelson, M. I.; Eaves, L.; Morozov, S. V.; Peres, N. M. R.; Leist, J.; Geim, A. K.; Novoselov, K. S.; Ponomarenko, L. A. Field-Effect Tunneling Transistor based on Vertical Graphene Heterostructures. *Science* **2012**, *335*, 947−950.
(11) Yim, C.; McEnoy, N.; Duesberg, G. S. Characterization of Graphene-Silicon Schottky Barrier Diodes Using Impedance Spectroscopy. *Appl. Phys. Lett.* **2013**, *103*, 193106.
(12) Tongay, S.; Schumann, T.; Hebard, A. F. Graphite based Schottky Diodes Formed on Si, GaAs, and 4H-SiC Substrates. *Appl. Phys. Lett.* **2009**, *95*, 222103.
(13) Chen, C.-C.; Akyol, M.; Chang, C.-C.; Levi, A. F. J.; Cronin, S. B. Graphene-Silicon Schottky Diodes. *Nano Lett.* **2011**, *11*, 1863−1867.
(14) Lin, Y.-J.; Lin, J.-H. Annealing Effect on Schottky Barrier Inhomogeneity of Graphene/n- type Si Schottky Diodes. *Appl. Surf. Sci.* **2014**, *311*, 224−229.
(15) Song, W.; Kim, Y.; Kim, S. H.; Kim, S. Y.; Cha, M.-J.; Song, I.; Jung, D. S.; Jeon, C.; Lim, T.; Lee, S.; Ju, S.; Choi, W. C.; Jung, M. W.; An, K.-S.; Park, C.-Y. Homogeneous and Stable p-Type Doping of Graphene by MeV Electron Beam-Stimulated Hybridization with ZnO Thin Films. *Appl. Phys. Lett.* **2013**, *102*, 053103.
(16) Zhang, Z.; Yao, K.; Liu, Y.; Jin, C.; Liang, X.; Chen, Q.; Peng, L.-M. Quantitative Analysis of Current−Voltage Characteristics of Semiconducting Nanowires: Decoupling of Contact Effects. *Adv. Funct. Mater.* **2007**, *17*, 2478−2489.
(17) Padovani, F. A.; Stratton, R. Field and Thermionic-Field Emission in Schottky Barriers. *Solid-State Electron.* **1966**, *9*, 695−707.
(18) Saxena, A. N. Forward Current-Voltage Characteristics of Schottky Barriers on n-type Silicon. *Surf. Sci.* **1969**, *13*, 151−171.
(19) Sinha, D.; Lee, J. U. Ideal Graphene/Silicon Schottky Junction Diodes. *Nano Lett.* **2014**, *14*, 4660−4664.
(20) Nie, B.; Hu, J.-G.; Luo, L.-B.; Xie, C.; Zeng, L.-H.; Lv, P.; Li, F.-Z.; Jie, J.-S.; Feng, M.; Wu, C.-Y.; Yu, Y.-Q.; Yu, S.-H. Monolayer Graphene Film on ZnO Nanorod Array for High-Performance Schottky Junction Ultraviolet Photodetectors. *Small* **2013**, *9*, 2872−2879.
(21) Xu, Q.; Cheng, Q.; Zhong, J.; Cai, W.; Zhang, Z.; Wu, Z.; Zhang, F. A Metal− Semiconductor−Metal Detector based on ZnO Nanowires Grown on a Graphene Layer. *Nanotechnology* **2014**, *25*, 055501.
(22) Fu, X.-W.; Liao, Z.-M.; Zhou, Y.-B.; Wu, H.-C.; Bie, Y.-Q.; Xu, J.; Yu, D.-P. Graphene/ZnO Nanowire/Graphene Vertical Structure based Fast-Response Ultraviolet Photodetector. *Appl. Phys. Lett.* **2012**, *100*, 223114.
(23) Kim, S.; Janes, D. B.; Choi, S.-Y.; Ju, S. Nanoscale Contacts between Semiconducting Nanowires and Metallic Graphenes. *Appl. Phys. Lett.* **2012**, *101*, 063122.

DOI: 10.1021/acsami.5b03380
ACS Appl. Mater. Interfaces 2015, 7, 18300−18305